

Feedback in AGN heating of galaxy clusters

M. Hoeft

M. Brüggen

International University Bremen

ABSTRACT

One of the challenges that models of AGN heating of the intracluster medium (ICM) face, is the question how the mechanical luminosity of the AGN is tuned to the radiative losses of the ICM. Here we implement a simple 1D model of a feedback mechanism that links the luminosity of the AGN to the accretion rate. We demonstrate how this simple feedback mechanism leads to a quasi-steady state for a broad range of parameters. Moreover, within this feedback model, we investigate the effect of thermal conduction and find that its relative importance depends strongly on the cluster mass.

Subject headings: galaxies: clusters: general, galaxies: active, X-ray: galaxies: clusters

1. Introduction

Currently, the most popular model that is invoked to explain the dearth of gas below about 1 keV in the ICM relies on the heating by a central AGN (Binney & Tabor 1995, Tabor & Binney 1993, Churazov et al. 2001, Brüggen & Kaiser 2002, Brüggen et al. 2002 Reynolds et al. 2001). Numerous observations of x-ray deficient bubbles in clusters and of motions induced by these bubbles have substantiated this model (e.g. Fabian et al. 2003, Mazzotta et al. 2002, Saxton et al. 2001, McNamara et al. 2001, Blanton et al. 2001). On the theoretical side, the efficiencies with which bubbles heat the ICM has been investigated, both numerically and analytically. E.g. Ruszkowski et al. (2004) found that up to 50 % of the internal energy of these bubbles is dissipated through viscous dissipation of waves and pdV work. The heating profile caused by bubbles has been parametrized

in a prescription named ‘effervescent heating’ by Begelman (2001), which will be used later in this paper.

However, one of the challenges that models of AGN heating face, is the question how the mechanical luminosity of the AGN is fine-tuned to the radiative losses of the ICM. If AGN heating is responsible for a diminution of the mass deposition rate in a whole range of clusters, the AGN needs to be regulated by the ICM itself. It has been suggested by some authors that AGN feedback may play a crucial role in self-regulating cooling flows (e.g. Churazov et al. 2002, Ruszkowski & Begelman 2002, Brighenti & Mathews 2003).

In this paper we present a simple model by which the central AGN adjusts its luminosity. This model assumes that the mechanical luminosity of the AGN is proportional to the accretion rate onto the AGN. In this picture, a very luminous central source will lead to a decrease in the accretion rate and hence also to a decline of the luminosity until, eventually, the cluster reaches a quasi-steady state. With the aid of a spherically

¹Campusring 1, 28759 Bremen, Germany

²An der Sternwarte 16, 14482 Potsdam, Germany

³mhoeft@iu-bremen.de

symmetric 1D model we study under which circumstances a self-regulated cooling flow is established. For feedback to be a viable model, the parameters of this model should not need any tuning.

In the following we will describe our initial models, our computational method and the implementation of feedback in more detail. Then, in section 4, we will present and discuss our results.

2. Model

2.1. Initial profiles

The initial cluster profiles are computed within the present canonical cosmological parameters, see Tab. 1. For the dark matter density distribution we assume an NFW profile given by (Navarro et al. 1996)

$$\rho_{\text{dm}} = \delta_c r^{-1} (r_s + r)^{-2}, \quad (1)$$

where δ_c is the characteristic density parameter and r_s the scaling radius. Thus, a cluster model is characterized by the virial mass M_{vir} and by the concentration parameter $c = r_s/r_{\text{vir}}$. Note, that the virial radius can be derived from $4/3 \pi r_{\text{vir}}^3 h^2 \rho_{\text{crit}} \Delta_c = M_{\text{vir}}$, where ρ_{crit} is the critical density and the density contrast Δ_c can be approximated by $\Delta_c = 178 \Omega_0^{0.45}$ (Eke et al. 1998).

Unlike for dark matter distributions, there is no universal profile for the intracluster gas. Here, we follow Roychowdhury et al. (2004) and assume that the initial temperature distribution is given by (Loken et al. (2002))

$$T_{\text{initial}}(r) = 1.3 T_{\text{ew}} (1 + 1.5 r/r_{\text{vir}})^{-1.6}. \quad (2)$$

Now, the emission-weighted X-ray temperature, T_{ew} , is known to scale with the cluster mass. Here, we adopt the $T_X - M$ -relation by Sanderson et al. (2003) who have analysed a large sample of virialized systems:

$$M_{200} = 2.34 \times 10^{13} M_{\odot} \left(\frac{k_B T_{\text{ew}}}{1 \text{ keV}} \right)^{1.84}. \quad (3)$$

Moreover, we assume that the gas is in hydrostatic equilibrium, i.e. the pressure force is balanced by gravitation

$$\frac{1}{\rho_{\text{gas}}} \frac{dP}{dr} = -\frac{GM_{\text{total}}(< r)}{r^2}, \quad (4)$$

where G is the gravitational constant and $M_{\text{total}}(< r)$ is the total cumulative mass up to r . We can express the pressure as $P = nk_B T$, where n is the particle number density, which is given for a fully ionized gas of primordial composition by $n = n_{\text{HII}} + n_{\text{HeIII}} + n_e = n_{\text{H}}(8 - 5Y_{\text{He}})/(4 - 4Y_{\text{He}})$, where Y_{He} is the Helium mass fraction. Since we assume an initial temperature profile, we can rewrite Eq. (4) and solve for the Hydrogen density n_{H}

$$\frac{dn_{\text{H}}}{dr} = -\frac{n_{\text{H}}}{T} \left\{ \frac{\mu m_{\text{H}}}{k_B} \frac{1}{r^2} M(< r) + \frac{dT}{dr} \right\}, \quad (5)$$

where the mean molecular weight is given by $\mu = 4/(8 - 5Y_{\text{He}})$. We integrate Eq. (5) subject to the condition that at radius r_{200} the ratio of the cumulative masses $M_{\text{gas}}/M_{\text{dm}}$ is equal to the cosmological value $\Omega_B/(\Omega_0 - \Omega_B)$.

2.2. Time integration

The entropy index $\sigma = T/n_e^{2/3}$ at a given radius evolves with time according to

$$\frac{d\sigma(r)}{dt} = \sigma(r) \frac{2}{3} \frac{1}{P(r)} \{ \mathcal{H}(r) - \Gamma(r) \}, \quad (6)$$

where $\mathcal{H}(r)$ denotes the total heating and $\Gamma(r)$ the cooling rate. For the subsequent calculations it is convenient to express the entropy profile as a function of the total enclosed mass, i.e. $\sigma = \sigma(M)$. Starting from an initial entropy profile that is calculated from the models described above, the cluster is evolved in time.

After each time step, Δt , the new profiles are calculated in two steps: first we calculate the change of entropy subject to heating and cooling, i.e.

$$\sigma \rightarrow \sigma + \frac{d\sigma(r)}{dt} \Delta t. \quad (7)$$

In the second step we calculate the new hydrostatic equilibrium into which the halo settles by solving

$$\begin{aligned} \frac{dr}{dM} &= \frac{1}{4\pi r^2 \rho_{\text{gas}}(r)} = \frac{1}{4\pi r^2} \left(\frac{\sigma}{P} \right)^{1/\gamma} \\ \frac{dP}{dM} &= -\frac{GM_{\text{total}}(< r)}{4\pi r^4}. \end{aligned} \quad (8)$$

Equations (8) are discretized on a non-uniform grid. A fine grid covers the inner region of the cluster out to a mass that in the initial model corresponds to a radius of $5 \times 10^{-2} r_{\text{vir}}$ and a coarser grid that covers the outer region out to r_{200} . Thus, the mass of a shell in the finely resolved region is 0.1% of the cumulative mass $M_{\text{gas}}(< r)$ compared to 2% in the coarse region. This results in about 4000 mass shells altogether.

Equation (8) is solved subject to the boundary condition that the pressure at r_{200} remains constant during the entire evolution, i.e. $P(r_{200}) = P_{200}$. In practice, we solve the system of coupled differential equations (8) subject to the initial conditions:

$$\begin{aligned} M(0) &= 0 \\ P(0) &= P_0, \end{aligned} \quad (9)$$

where P_0 is a trial value which is varied until the pressure at r_{200} is equal to the specified pressure P_{200} . Note that this implies that the radius r_{200} changes in the course of time as the cluster expands and contracts.

2.3. Radiative cooling and conduction

In the temperature range that we are mainly interested in, namely between $10^5 - 10^8$ K, radiative cooling is dominated by free-free emission. For a fully ionized plasma the cooling rate can be approximated by (Katz et al. 1996)

$$\Lambda_{\text{free-free}} = 1.42 \times 10^{-27} g_{\text{ff}} T^{1/2} (n_{\text{H}} + 4n_{\text{He}}) n_e \frac{\text{erg}}{\text{s cm}^3}, \quad (10)$$

with the Gaunt factor

$$g_{\text{ff}} = 1.1 + 0.34 \exp\{-(5.5 - \log T)^2/3\}. \quad (11)$$

In addition we consider metal-dependent cooling, which we approximate crudely following Theis et al. (1992)

$$\begin{aligned} \Lambda_{\text{metal}} &= 10^{-22-5m(Z)+7\sqrt{Z}} T^{m(Z)} n_{\text{H}}^2 \frac{\text{erg}}{\text{s cm}^3} \\ m(Z) &= \frac{2.5 + 7\sqrt{Z}}{5 - \log(1.48 \times 10^{11} Z^{1.1} + 10^6)}, \end{aligned} \quad (12)$$

where Z denotes the mass fraction of metals. Here we assume $Z = 0.3 Z_{\odot}$ and we limit the cooling

in the core by assuming a minimum entropy index $\sigma_{\text{min}} = 10^{-2} \text{ keV cm}^2$.

The role of thermal conduction in the ICM has been the subject of a long debate and, owing to the complex physics of MHD turbulence, the value of the effective conductivity remains uncertain. The thermal conductivity of an unmagnetised, fully ionised plasma was calculated by Spitzer (1962). Originally it was thought that the magnetic field in clusters strongly suppressed the thermal conductivity because the magnetic fields prevented an efficient transport perpendicular to the field lines. Even if the transport can be efficient along the magnetic field lines, the overall isotropic conductivity was thought to be many orders of magnitude less than the Spitzer value. This paradigm has been supported by a number of observations, such as sharp edges at so-called cold fronts and small-scale temperature variations (Markevitch et al. 2000, Vikhlinin et al. 2001).

Recent theoretical work by Narayan & Medvedev (2001), Chandran et al. (1999), Chandran & Cowley (1998) and earlier work by Rechester & Rosenbluth (1978) have shown that a turbulent magnetic field is not as efficient in suppressing thermal conduction as previously thought. It is argued that chaotic transverse motions of the tangled magnetic field lines can enhance the cross-field diffusion to an extent that the effective conductivity is of the order of the Spitzer value. Thus, we decided to investigate the effects of thermal conduction within our feedback model. Recently, the role of thermal conduction in clusters was also investigated numerically by Dolag et al. (2004) and Jubelgas et al. (2004).

The energy flux due to thermal conduction is given by

$$F_{\text{cond}} = -\kappa \nabla T, \quad (13)$$

where κ is the coefficient of thermal conductivity which we assume to be a fraction f of the Spitzer conductivity

$$\kappa_0 T^{5/2} \approx 5 \times 10^{-7} T^{5/2} \frac{\text{erg}}{\text{s cm K}}. \quad (14)$$

Under the assumption of spherical symmetry, the heating and cooling rate due to thermal conduc-

tion become

$$\begin{aligned}\Gamma_{\text{cond}} &= -\frac{1}{r^2} \frac{d}{dr} \{r^2 F_{\text{cond}}\} \\ &= -f_{\text{Spitz}} \kappa_0 \frac{T^{3/2}}{r} \left\{ 2T \frac{dT}{dr} + \frac{5}{2} r \left(\frac{dT}{dr} \right)^2 + rT \frac{d^2 T}{dr^2} \right\}\end{aligned}$$

The timestepping in the integration of Eq. (8) is constrained by the appropriate Courant condition (Ruszkowski & Begelman 2002). The most restrictive term comes from thermal conduction which can be obtained from a von Neumann stability analysis, i.e.

$$\Delta t = \frac{3k_B n (\Delta r)^2}{4f_{\text{Spitz}} \kappa_0 T^{5/2}}, \quad (16)$$

where Δr denotes the local spatial resolution. The time step obviously changes in the course of the simulation but for our resolution a typical time step is of the order of 0.05 Myr.

Since we do not use a uniform grid, especially with respect to the spatial spacing, we compute the derivatives of the temperature by a local polynomial fit. Around each point in radius we expand the temperature to second order

$$T(r) = T(r_0) + \frac{dT}{dr}(r - r_0) + \frac{1}{2} \frac{d^2 T}{dr^2} (r - r_0)^2 \quad (17)$$

and approximate the derivatives with a weighted least-square regression. We solve the equation

$$\mathbf{Q} = \mathbf{W} \cdot \begin{pmatrix} T(r_0) \\ dT/dr \\ 1/2 d^2 T/dr^2 \end{pmatrix} \quad (18)$$

where

$$\begin{aligned}Q_i &= \sum_n T_n \omega_n (r_n - r_0)^i \\ W_{ij} &= \sum_n \omega_n (r_n - r_0)^{i+j}.\end{aligned} \quad (19)$$

The sum is taken over all sampling points n and $i, j \in \{0, 1, 2\}$. The weights are given by

$$\omega_n = \begin{cases} (r_n - r_{n-1}) e^{-4(r_n - r_0)^2 / \Delta^2} & : |r_n - r_0| < 2\Delta \\ 0 & : \text{otherwise} \end{cases} \quad (20)$$

For the smoothing length we take $\Delta = \max\{0.05 \times r, 0.05 \text{ kpc}\}$. Finally, we neglected convection which proved to be virtually irrelevant for our simulations since the entropy remained monotonous even in the presence of strong heating.

2.4. Heating and feedback

In the centres of clusters active galactic nuclei inflate buoyant bubbles of relativistic gas which release some of their internal energy by pdV -work on the ambient medium. This work is done as the bubbles expand on their ascent through the stratified cluster medium. Churazov et al. (2001) and Begelman (2001) have calculated this work and found that the heat released by one bubble is given by

$$h(r) \propto P^{(\gamma_b - 1)/\gamma_b} \frac{1}{r} \frac{d \ln P}{d \ln r}. \quad (21)$$

Under the assumption of spherical symmetry the heat has to be distributed over spherical shells, which introduces a geometric factor $f_{\text{geom}} \propto 1 / 4\pi r^2$. However, at radii smaller than a typical bubble diameter this argument does not hold. In the center we assume that the heating is given by the heating function of one bubble, therefore we cut off the geometrical factor below the typical bubble size d_{bubble} , by changing $f_{\text{geom}}: r^2 \rightarrow r^2 + d_{\text{bubble}}^2$. As bubbles rise through the ICM they are likely to be disrupted by Rayleigh-Taylor instabilities. The smaller fragments rise more slowly and are disrupted more easily until they virtually stop. As a result the effervescent heating rate is effectively cut off at the periphery of the cluster. This effect is approximated by introducing a factor $\exp\{-(r/r_{\text{disr}})\}$, where the disruption radius, r_{disr} , is set to 0.5 Mpc. We note, however, that this cut-off at large radii only has a mild effect on our simulations and is not strictly necessary. Thus the effervescent heating rate is given by

$$\mathcal{H}(t) = \mathcal{L}_{\text{eff}}(t) h(r) f_{\text{geom}}(r), \quad (22)$$

where the radially dependent functions are normalized according to

$$\int_{r_{\text{min}}}^{r_{\text{max}}} dr 4\pi r^2 h(r) f_{\text{geom}}(r) = 1. \quad (23)$$

The geometrical factor is given by

$$f_{\text{geom}}(r) = \frac{\exp\{-(r/r_{\text{disr}})\}}{4\pi(r^2 + d_{\text{bubble}}^2)}, \quad (24)$$

and $\mathcal{L}_{\text{eff}}(t)$ denotes the total ‘effervescent’ luminosity at time t .

In our continuous feedback model we assume that the luminosity of the AGN is proportional to the mass accretion onto the core, i.e.

$$\mathcal{L}_{\text{eff}}(t) = \epsilon \dot{M}_{\text{core}} c^2, \quad (25)$$

where the core is made up of gas whose entropy index lies below a minimal value, σ_{min} .

The accretion rate is calculated by a linearly weighted least-square regression of the function $M_{\text{core}}(t)$, where a similar procedure as described in Sec. 2.3 is used with a smoothing timescale of 20 Myr. In order to improve numerical stability we introduce a delay time of 2 Myr, i.e. the luminosity is proportional to the accretion rate of 2 Myr ago.

3. Results

3.1. Self-regulated luminosities

As our canonical model we take a cluster with a dark matter mass of $M_{\text{vir}} = 4 \times 10^{14} M_{\odot}$ and a concentration parameter $c = 4$. These values are chosen to resemble those of the cooling flow cluster Abell 2052 (Blanton et al. 2003). We start all our simulations from the initial temperature profile given by Eq. (2) and leave conduction and heating switched off until the cluster has formed a cold core. Only then we begin with the simulation of feedback.

As the ICM cools and the central cooling times decrease, the accretion onto the core increases and so does, according to our prescription for feedback, the luminosity of the AGN. We will start by first describing the simulation without thermal conduction.

Fig. 1 shows the self-regulated luminosity of the effervescent heating as a function of time for various values of the efficiency, ϵ . After an initial phase which only lasts for a few hundred Myrs the luminosity converges to a value of around $L \sim 10^{44}$ erg s⁻¹ and remains steady for the entire length of the simulation, which is longer than 3 Gyrs. Runs

with different efficiencies show, that the effervescent heating is in fact the regulating parameter. Even for quite different efficiencies that span two orders of magnitude the luminosities end up at quite similar values.

The heating stalls the accretion onto the core as is shown in Fig. 2 which shows the accretion rate as a function of time. One can see how the accretion rate adjusts itself to a value just below $1 M_{\odot}/\text{yr}$ after a few hundred Myrs. For comparison we also show the corresponding scenario with neither heating nor conduction by the thick double-dashed line that is labelled by “all off”. It shows how quickly the accretion rate diverges in the absence of heating.

Many AGN are believed to be recurrent with duty cycles between 10 and a few 100 Myrs. This suggests that a non-linear feedback process is at work, i.e. that the luminosity is not linearly related to the accretion rate as presumed here. However, nothing is known about the parameters of such a non-linear feedback mechanism. One could, for instance, introduce upper and lower thresholds for \dot{M} , such that the AGN switches on if the accretion rate lies above the upper threshold and is switched off when it falls below the lower threshold. Depending on the values for these thresholds one can reproduce sensible duty cycles, but since one has introduced two more parameters, this is no great achievement. Therefore, we decided to focus on a simple prescription for continuous feedback which introduces only a single parameter. Most importantly, our results depend only very weakly on this parameter. Furthermore, even if in nature feedback operates in some non-linear fashion, our results are still valid in a time-averaged (i.e. averaged over a few duty cycles) sense since the recurrence times are small compared to the time scales considered here. Thus, if the AGN is active for only part of the time, the mechanical luminosities of the central AGN can be higher than the $\sim 10^{44}$ erg s⁻¹ found here.

3.2. The effect of conduction

Next, we studied the effects of thermal conduction on our models. Fig. 3 is the corresponding plot to Fig. 1 with thermal conduction (where we assumed $f = 0.3$). The solid lines in Figs. 1 and 3 both correspond to the same efficiency of 3×10^{-3} and it is evident that the presence of thermal conduction leads to decrease of the accretion rates and, consequently, also of the effervescent luminosities. Initially, i.e. after about 500 Myrs, the luminosities are very similar at $\sim 10^{44}$ erg s $^{-1}$ but at later times thermal conduction suppresses the luminosities to less than $\sim 10^{43}$ erg s $^{-1}$. Higher efficiencies reduce the power of the AGN even further, while efficiencies of around 3×10^{-4} result in a very steady luminosity. In any case, for a wide range of efficiencies we obtain cluster models that remain stable over long times and require 'effervescent' luminosities of not more than $\sim 10^{44}$ erg s $^{-1}$.

Fig. 4 shows the volume heating and cooling rates of our simulations of clusters with masses of $10^{14} M_{\odot}$, $4 \times 10^{14} M_{\odot}$ and $10^{15} M_{\odot}$ with an efficiency parameter of $\epsilon = 3 \times 10^{-3}$ and an assumed conductivity of 30% of the Spitzer conductivity ($f = 0.3$). The figure shows the curves at a time of 1 Gyr after the start of the feedback. The solid line shows the radial cooling profile, while the double-dashed line shows the effervescent heating rate. It is evident from the left panel that for the cluster with a mass of $10^{14} M_{\odot}$ the radiative cooling is almost exactly balanced by the effervescent heating while conduction has very little effect on the energy budget. Also note, that thermal conduction can, both, heat and cool the cluster as is shown by different lines in Fig. 4. In the outer regions and at the edge of the core, conduction leads to cooling while regions between a few kpc to ~ 100 kpc are heated. This has also been inferred from observations of M87 (Ghizzardi et al. 2004). In the very center the heating due to conduction drops to small values since the temperature is very low. However, the relative importance of conduction increases with mass. This is not unexpected since the thermal conductivity depends

strongly on temperature and temperature scales with mass. For the cluster with $M = 4 \times 10^{14} M_{\odot}$ conduction is already more important than effervescent heating for most regions within the cluster. Especially conduction can heat the region around the core and thus effectively suppresses the accretion. The figure shows that conduction alone almost compensates the radiative cooling, particularly in regions where the bulk of X-ray emission comes from. This is in agreement with previous findings e.g. by Narayan & Medvedev (2001) and Fabian et al. (2002).

3.3. Comparisons with observations

While we do not intend to undertake a thorough modelling of the observed features of cooling flow clusters, it is still essential to verify whether our model can reproduce the gross features of typical cooling flow clusters.

Fig. 5 shows the temperature profiles for a model with $M_{\text{vir}} = 4 \times 10^{14} M_{\odot}$ and $c = 4.0$ at different times. Mass and concentration parameter are chosen to lie close to the values of Abell 2052, which is a well known cooling flow cluster. The initial temperature profile is fairly flat as shown by the top curve in Fig. 5, but slowly the central temperature drops and after about 9 Gyrs a cold core has formed. The symbols in Fig. 5 denote the observed temperatures for A 2052 (Blanton et al. 2003). We note that the data are consistent with our model at late times, i.e. after the formation of the core. Especially the slopes within 50 kpc agree nicely, whereas in the outer regions the observations show higher temperatures than our model. This may be an indication that in the periphery other heating processes are at work. Given the simplicity of our model, it may be imprudent to overstretch its similarity with observations but in any case it is encouraging that the profiles that we obtain are not disparate from observations. Again, we wish to stress that the temperature profiles are quite insensitive to the efficiency of the feedback.

Finally, it is interesting to compare our accretion rates to the accretion rates inferred from the total x-ray luminosity according to the classical

cooling flow model, given by

$$\dot{M}_{\text{cool-flow}} \approx \frac{2}{5} \frac{\mu m_{\text{H}}}{k_B T_X} L_X (< r_c), \quad (26)$$

where r_c is the cooling radius at which $t_c \approx H_0^{-1}$ and L_X is the bolometric x-ray luminosity. Fig. 6 shows the inferred mass deposition rates for some of our simulated clusters. Comparing $\dot{M}_{\text{cool-flow}}$ to \dot{M}_{core} reveals that the accretion rates inferred from the X-ray emission are considerably higher than the rates derived from our single-phase model. In the presence of heating, the simple equation for $\dot{M}_{\text{cool-flow}}$ overestimates the accretion onto the core at least by a factor of 10. The reason is, of course, that the radiative losses are replenished by bubble heating and thermal conduction, and thus unaccounted for in Eq. (26). Again, the variation of $\dot{M}_{\text{cool-flow}}$ with ϵ is relatively weak. To put this variation into perspective we show how much more strongly $\dot{M}_{\text{cool-flow}}$ depends on the concentration parameter (top curve in Fig. 6) when all other parameters remain the same.

3.4. Summary

We found that a simple prescription for feedback leads to a self-regulated steady-state model for the ICM: For a wide range of efficiencies the self-regulated luminosities lie around $L \sim 10^{44}$ erg/s which corresponds to a mass accretion rate of $\dot{M} \sim 1M_{\odot}/\text{yr}$. Thermal conduction decreases the luminosity in a self-regulated model and is the more important the more massive the cluster is.

The resulting profiles for temperature are consistent with observations of cooling flow clusters. In the presence of heating, the classical cooling flow model grossly overestimates the mass deposition rates.

ACKNOWLEDGEMENT

The authors wish to thank Mateusz Ruszkowski and Eugene Churazov for many helpful suggestions and Sebastian Heinz for his early involvement in the project. Support by DFG through grant BR 2026/2 is gratefully acknowledged. The

calculations were performed at the CLAMV at the International University Bremen.

REFERENCES

- Begelman, M. C. 2001, in ASP Conf. Ser. 240: Gas and Galaxy Evolution, 363–+
- Binney, J. & Tabor, G. 1995, MNRAS, 276, 663
- Blanton, E. L., Sarazin, C. L., & McNamara, B. R. 2003, ApJ, 585, 227
- Blanton, E. L., Sarazin, C. L., McNamara, B. R., & Wise, M. W. 2001, ApJ, 558, L15
- Brüggen, M., Kaiser, C. R., Churazov, E., & Enßlin, T. A. 2002, MNRAS, 331, 545
- Brighenti, F. & Mathews, W. G. 2003, ApJ, 587, 580
- Brüggen, M. & Kaiser, C. R. 2002, Nature, 418, 301
- Chandran, B. D. G. & Cowley, S. C. 1998, Physical Review Letters, 80, 3077
- Chandran, B. D. G., Cowley, S. C., Ivanushkina, M., & Sydora, R. 1999, ApJ, 525, 638
- Churazov, E., Brüggen, M., Kaiser, C. R., Böhringer, H., & Forman, W. 2001, ApJ, 554, 261
- Churazov, E., Sunyaev, R., Forman, W., & Böhringer, H. 2002, MNRAS, 332, 729
- Dolag, K., Jubelgas, M., Springel, V., Borgani, S., & Rasia, E. 2004, ApJ, 606, L97
- Eke, V. R., Navarro, J. F., & Frenk, C. S. 1998, ApJ, 503, 569
- Fabian, A. C., Sanders, J. S., Allen, S. W., Crawford, C. S., Iwasawa, K., Johnstone, R. M., Schmidt, R. W., & Taylor, G. B. 2003, MNRAS, 344, L43
- Fabian, A. C., Voigt, L. M., & Morris, R. G. 2002, MNRAS, 335, L71

- Ghizzardi, S., Molendi, S., Pizzolato, F., & de Grandi, S. 2004, ArXiv Astrophysics e-prints
- Jubelgas, M., Springel, V., & Dolag, K. 2004, MNRAS, 5
- Katz, N., Weinberg, D. H., & Hernquist, L. 1996, ApJS, 105, 19
- Loken, C., Norman, M. L., Nelson, E., Burns, J., Bryan, G. L., & Motl, P. 2002, ApJ, 579, 571
- Markevitch, M., Ponman, T. J., Nulsen, P. E. J., Bautz, M. W., Burke, D. J., David, L. P., Davis, D., Donnelly, R. H., Forman, W. R., Jones, C., Kaastra, J., Kellogg, E., Kim, D.-W., Kolodziejczak, J., Mazzotta, P., Pagliaro, A., Patel, S., Van Speybroeck, L., Vikhlinin, A., Vrtilik, J., Wise, M., & Zhao, P. 2000, ApJ, 541, 542
- Mazzotta, P., Kaastra, J. S., Paerels, F. B., Ferrigno, C., Colafrancesco, S., Mewe, R., & Forman, W. R. 2002, ApJ, 567, L37
- McNamara, B. R., Wise, M. W., Nulsen, P. E. J., David, L. P., Carilli, C. L., Sarazin, C. L., O’Dea, C. P., Houck, J., Donahue, M., Baum, S., Voit, M., O’Connell, R. W., & Koekemoer, A. 2001, ApJ, 562, L149
- Narayan, R. & Medvedev, M. V. 2001, ApJ, 562, L129
- Navarro, J. F., Frenk, C. S., & White, S. D. M. 1996, ApJ, 462, 563
- Rechester, A. B. & Rosenbluth, M. N. 1978, Physical Review Letters, 40, 38
- Reynolds, C. S., Heinz, S., & Begelman, M. C. 2001, ApJ, 549, L179
- Roychowdhury, S., Ruszkowski, M., Nath, B. B., & Begelman, M. C. 2004, ArXiv Astrophysics e-prints
- Ruszkowski, M. & Begelman, M. C. 2002, ApJ, 581, 223
- Ruszkowski, M., Bruggen, M., & Begelman, M. C. 2004, ArXiv Astrophysics e-prints
- Sanderson, A. J. R., Ponman, T. J., Finoguenov, A., Lloyd-Davies, E. J., & Markevitch, M. 2003, MNRAS, 340, 989
- Saxton, C. J., Sutherland, R. S., & Bicknell, G. V. 2001, ApJ, 563, 103
- Spitzer, L. 1962, Physics of Fully Ionized Gases (Physics of Fully Ionized Gases, New York: Interscience (2nd edition), 1962)
- Tabor, G. & Binney, J. 1993, MNRAS, 263, 323
- Theis, C., Burkert, A., & Hensler, G. 1992, A&A, 265, 465
- Vikhlinin, A., Markevitch, M., & Murray, S. S. 2001, ApJ, 551, 160

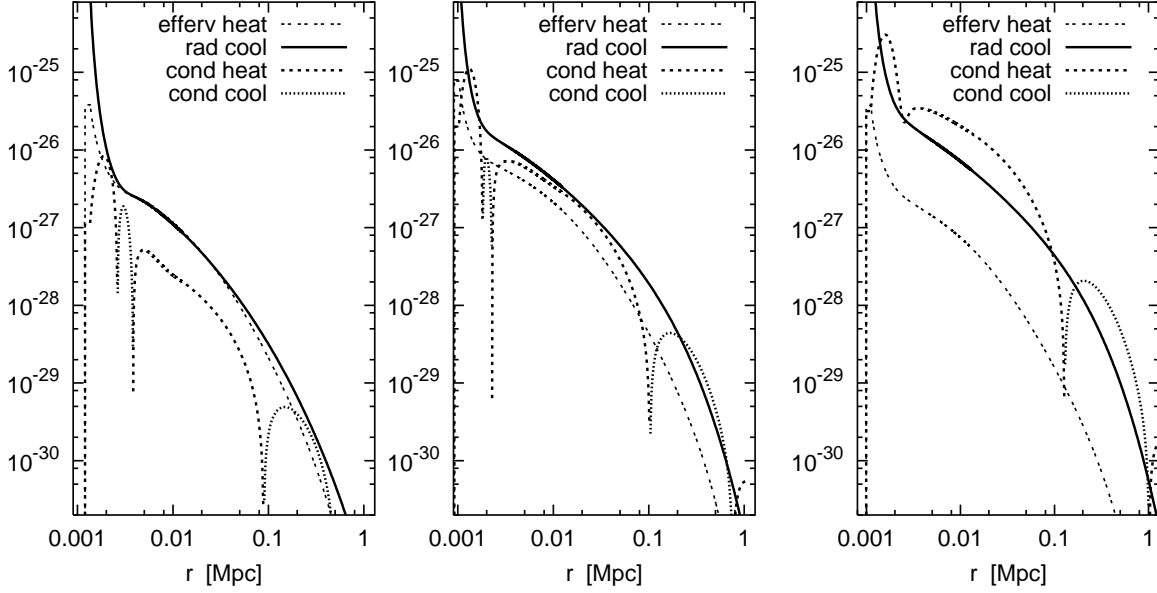


Fig. 4.— The volume heating and cooling rates for three models of different masses (from left to right the mass is $10^{14} M_{\odot}$, $4 \times 10^{14} M_{\odot}$ and $10^{15} M_{\odot}$; $c = 4$ for all models). The units on the vertical axis are $\text{erg cm}^{-3}\text{s}^{-1}$. All three figures correspond to a time of 1 Gyr after the AGN has been switched on. The feedback parameter is $\epsilon = 3 \times 10^{-3}$.

Cosmological model		
matter density	Ω_0	0.3
baryon density	Ω_B	0.04
Hubble constant	$h = H_0/H_0^{100}$	0.7
Helium mass fraction	Y_{He}	0.24
Dark matter halo		
dark matter virial mass *	M_{vir}	$10^{14} M_{\odot}$
concentration parameter *	c	4
Effervescent energy feedback		
efficiency *	ϵ	3×10^{-3}
initial bubble size	d_{bubble}	20 kpc
disruption radius	r_{disr}	500 kpc
Conduction		
Spitzer fraction *	f_{Spitz}	0.3

Table 1: Parameters used for our standard simulation. To study other cluster models parameters marked with * are varied.

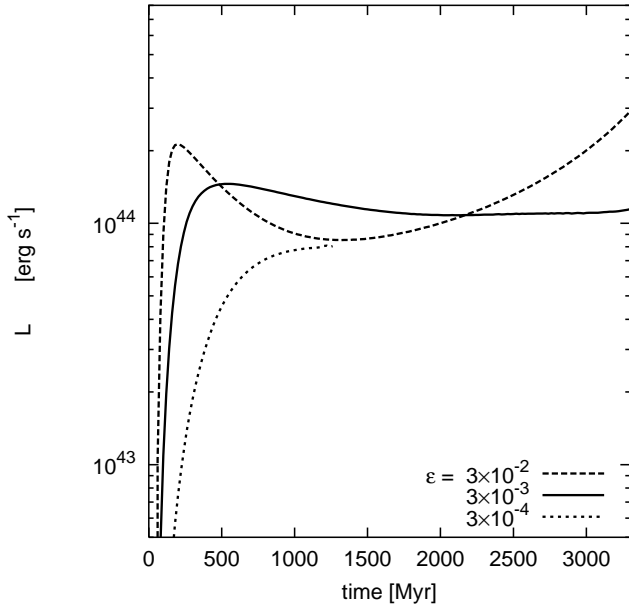


Fig. 1.— Luminosity of the effervescent heating as a function of time. The lines correspond to models with different efficiencies, ϵ . The oscillations that appear at late times for very low luminosities are numerical artefacts caused by the finite resolution of the mass shells.

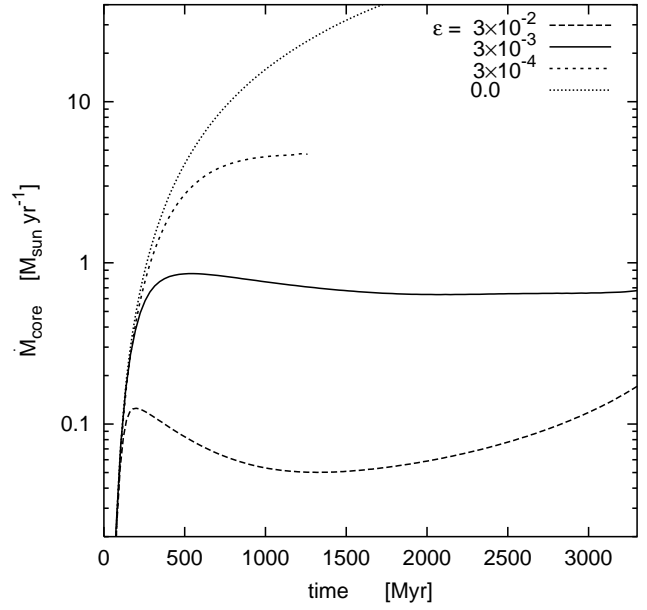


Fig. 2.— Mass accretion rate onto the core as a function of time. The lines correspond to models with different efficiencies, ϵ . The oscillations that appear at late times for very low luminosities are numerical artefacts caused by the finite resolution of the mass shells. The thick double-dashed line that is labelled by “all off” is the accretion rate in a model without heating. It shows how quickly the mass accretion rate diverges in the absence of heating.

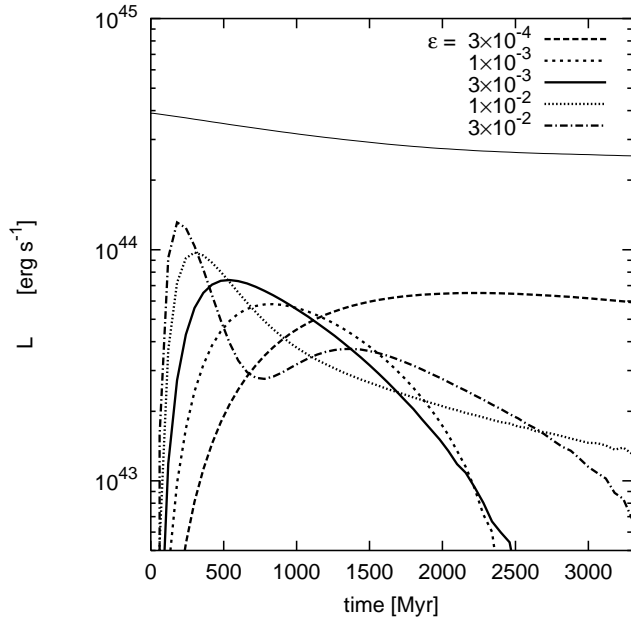


Fig. 3.— Same as Fig. 1 but with thermal conduction. For comparison, the thin line denotes the volume integrated radiative luminosity of the ICM as a function of time.

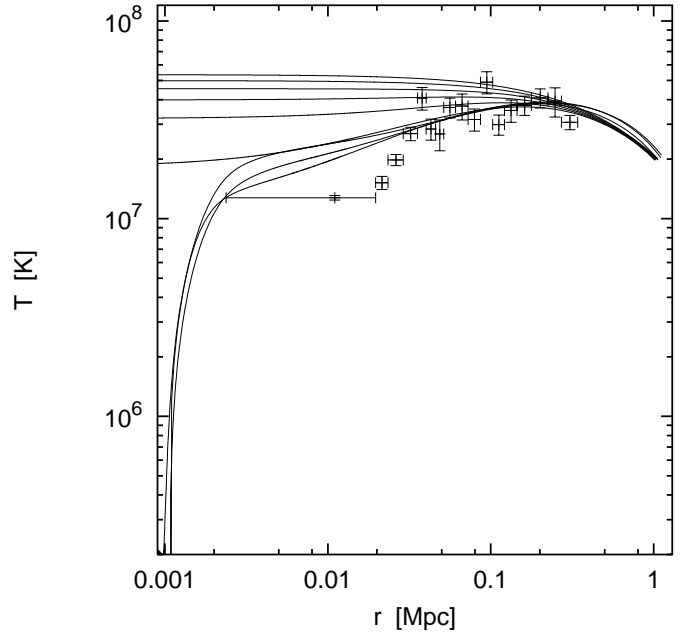


Fig. 5.— Temperature profiles for a cluster model with $M_{\text{vir}} = 4 \times 10^{14} M_{\odot}$ and $c = 4.0$. Mass and concentration are chosen close to the values of Abell 2052, which is a well known cooling flow cluster. The different lines correspond to different points in time with a new line drawn every 2 Gyr up to 16 Gyr. Symbols indicate the observed temperature profile (Blanton et al. 2003).

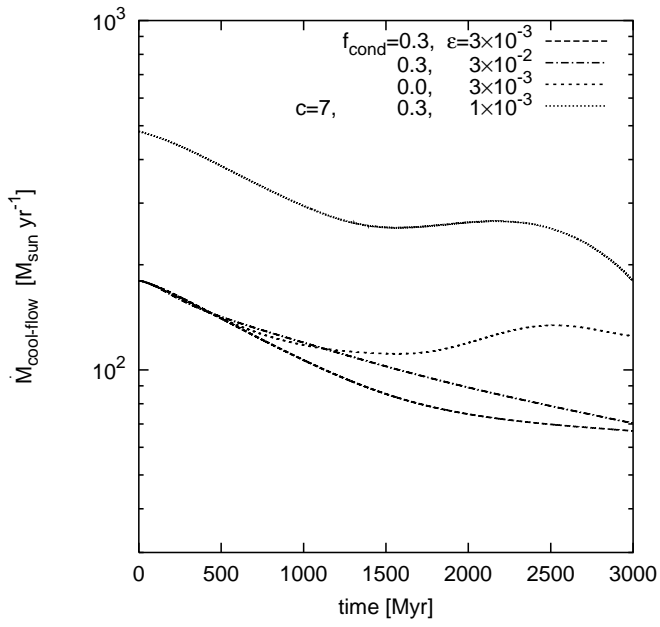


Fig. 6.— Mass deposition rates inferred according to the classical cooling flow model, i.e. Eq.(26). The dashed lines correspond to our canonical model ($M_{\text{vir}} = 4 \times 10^{14} M_{\odot}$ and $c = 4$) with different efficiencies and conductivities, while the dotted line corresponds to a model with $\epsilon = 10^{-3}$ but a higher concentration parameter ($c = 7$).